JACS
JOURNAL OF THE AMERICAN CHEMICAL SOCIETY
Communication
pubs.acs.org/JACS

Hematite/Si Nanowire Dual-Absorber System for Photoelectrochemical Water Splitting at Low Applied Potentials

Matthew T. Mayer, Chun Du, and Dunwei Wang*

Department of Chemistry, Merkert Chemistry Center, Boston College, Chestnut Hill, Massachusetts 02467, United States

Supporting Information

ABSTRACT: Hematite (α-Fe_2O_3) was grown on vertically aligned Si nanowires (NWs) using atomic layer deposition to form a dual-absorber system. Si NWs absorb photons that are transparent to hematite (600 nm < λ < 1100 nm) and convert the energy into additional photovoltage to assist photoelectrochemical (PEC) water splitting by hematite. Compared with hematite-only photoelectrodes, those with Si NWs exhibited a photocurrent turn-on potential as low as 0.6 V vs RHE. This result represents one of the lowest turn-on potentials observed for hematite-based PEC water splitting systems. It addresses a critical challenge of using hematite for PEC water splitting, namely, the fact that the band-edge positions are too positive for high-efficiency water splitting.

Photoelectrochemical (PEC) water splitting offers the capability of harvesting the energy in solar radiation and transferring it directly to chemical bonds for easy storage, transport, and use in the form of hydrogen.[1] Among the various considerations of a PEC system, the choice of photoelectrode materials is especially important because their properties, such as optical absorption characteristics and chemical stability, determine the system's performance. On the basis that these materials should absorb light broadly and be inexpensive and resistant to photocorrosion, hematite (α-Fe_2O_3) has emerged as a model material that has been studied extensively.[2] Much research has been devoted to combating the key challenges presented by hematite, including short hole diffusion distances[3] and poor catalytic activities.[4] More recently, we reported an approach addressing another critical challenge, namely, the mismatch of hematite band edge positions with the reduction and oxidation potentials of water, by forming buried n–p junctions.[5] In general, these existing efforts have rarely sought to utilize the portion of the solar spectrum that cannot be absorbed by hematite (λ > 600 nm), which accounts for more than half of the total solar energy. Here we show that red and near-IR photons (600 nm < λ < 1100 nm) can be readily collected to provide extra photovoltage when hematite is interfaced with Si nanowires (NWs). The resulting photoelectrode exhibits a photocurrent turn-on potential as low as 0.6 V vs reversible hydrogen electrode (V_{RHE}).

As illustrated in Figure 1a, the key idea is to employ two (or more) semiconductors that absorb in different regions of the solar spectrum. The first absorber, hematite, operates as a typical photoelectrode for water photooxidation, while the second one, the Si NW, uses the energy of long-wavelength photons to increase further the energy of electrons that will be ultimately utilized for water photoreduction. The net effect is that hematite-based water splitting can be carried out at reduced external potentials. This design is to be compared with that employing dye-sensitized solar cells (DSSCs) to augment hematite water splitting, where an extra device, the DSSC, is needed,[6] or the record-efficiency PEC/photovoltaic system demonstrated by Khaselev and Turner,[7] where the stability and cost of the electrode is a serious concern. The design is also different from the Si-based triple-junction photoelectrode recently demon-

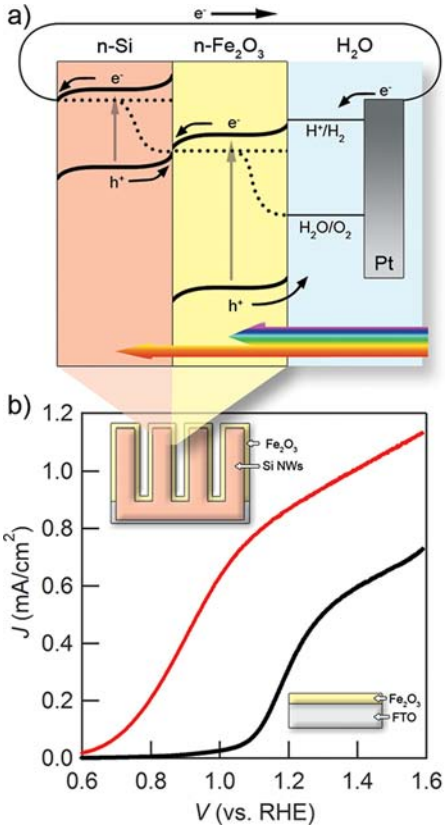

Figure 1. (a) Energy band schematics (quasi-static equilibrium under solar illumination) of the hematite/Si NW dual-absorber system. (b) *J*–*V* plots under simulated solar illumination (AM 1.5, 100 mW cm^{-2}) in 1.0 M NaOH aqueous electrolyte (scan rate 10 mV s^{-1}) for the Fe_2O_3/Si NW system (red) and Fe_2O_3 on planar FTO (black).

Received: May 28, 2012
Published: July 16, 2012

   dx.doi.org/10.1021/ja3051734 | *J. Am. Chem. Soc.* 2012, 134, 12406–12409

strated by Nocera and co-workers[8] because what we present here aims at solving fundamental challenges associated with hematite (which are also common for many other transition metal oxides), which is expected to exhibit superior stability against photocorrosion in comparison with Si. Notably, Yang and co-workers have demonstrated a similar concept on Si NW/TiO_2 combinations, where the authors emphasized the surface-area-induced photocurrent enhancement but not the cathodic shift of the photocurrent turn-on voltage.[9] We highlight that the experimental demonstration of the dual-absorber concept on hematite, enabled by our capability to grow high-quality metal oxides on textured surfaces (Si NWs) by atomic layer deposition (ALD), is new and that the results have significant implications.

Figure 1b compares plots of photocurrent density (J) versus applied potential (V) for hematite photoelectrodes with and without the second absorber of Si NWs. Most obvious is the significant shift of the curve in the cathodic direction. Because the two photoelectrodes were prepared from the same batch of hematite growth, we ruled out the possibilities of unintentional doping or other phenomenological surface effects such as passivation[10] or catalyst decoration.[11] A second artifact we considered was whether the current came from photocorrosion of Si, which would result from unsuccessful coverage of Si NWs by hematite. Electron microscopy studies revealed that the hematite layer was conformal (Figure 2 and Figure S1 in the Supporting Information). The crystalline nature of hematite was also confirmed by the electron diffraction pattern (Figure 2b inset). While n-type doping by Si has been shown to enhance the electron conductivity in hematite,[12] no appreciable Si concentration was detected in the hematite layer of our Fe_2O_3/Si NW devices, suggesting that negligible outward diffusion of Si into hematite took place during the mild postgrowth annealing treatment (500 °C). More important, a sustained photocurrent without decay was measured for up to 3 h of continued PEC reaction (Figure S2). If a significant portion of the measured current came from Si photocorrosion, a drastic decay of the photocurrent would be expected.[13] Taken together, the data show that the cathodic shift of the photocurrent in Figure 1b is indeed a result of additional photovoltage produced at the Fe_2O_3–Si junction by Si NWs.

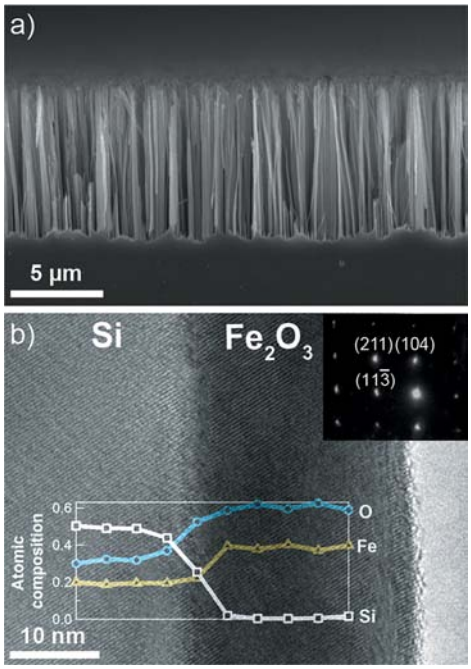

Figure 2. Microstructure of the Si/Fe_2O_3 NW photoelectrodes. (a) Scanning electron micrograph showing the arrangement of chemically etched Si NWs. (b) Transmission electron micrograph showing the crystalline quality of the Fe_2O_3 film grown on the Si NW surface by ALD. Insets: electron diffraction pattern (top right) and energy-dispersive X-ray spectroscopy line scans revealing the compositional makeup across the Si–Fe_2O_3 interface (bottom).

The working principle of the system (Figure 1a) predicts that the overall photocurrent should be limited by the lowest-performing component, which in the present case is hematite. Thus, unless the light absorption by hematite is significantly improved, a dramatic increase of photocurrent would not be expected. This prediction was verified by our experiments. When hematite was grown on planar Si substrates, low photocurrents were measured (Figure S3a). The higher photocurrent measured on the hematite/Si NW combination is a result of increased light absorption by hematite on the textured substrate (Si NWs) due to the enhanced path length for photon absorption and the increased surface area. This is similar to what has been demonstrated by us using $TiSi_2$ nanonets,[3c,14] although the enhancement is less significant here, presumably because of the compactness of the etched Si NWs. More precisely, we believe that dynamic electrolyte diffusion into and out of the regions between adjacent Si NWs is poor, since an electrochemically active effective surface-area-to-projected-area ratio of <2, which is 2 orders of magnitude lower than the true surface area, has been measured by us on Si NWs prepared by the same method in the Me_2Fc/Me_2Fc^+ electrochemical system.[15] Optimization of the Si nanostructure may further improve the photocurrent. Importantly, however, the cathodic shift in the J–V plots observed on the planar hematite/Si system (Figure S3a) was comparable to that in Figure 1b, supporting the conclusion that the proposed mechanism in Figure 1a is reasonable.

The band diagrams shown in Figure 1a and Figure S4 also predict that the magnitude of the cathodic shift should depend on how much photovoltage can be produced by the Si NWs, which in turn is determined by the extent of band bending within Si. One way to test this prediction would be to change the position of the Fermi level within Si by, for instance, using Si with different doping levels, doping type, or both. When the Fermi level is closer to the valence band (VB) edge (such as in p-type Si), the photovoltage obtained on Si is smaller, resulting in a smaller cathodic shift. Combined with the fact that an appreciable band-bending depth is necessary for charge separation, this indicates that a lightly n-doped Si would be desired for the dual-absorber system to exhibit the most significant cathodic shift. This indeed was the case. We examined Si n-doping levels of 10^{14}, 10^{16}, and 10^{18} cm^{-3}, which led to typical onset potentials of approximately 0.6, 0.8, and 0.9 V_{RHE}, respectively, whereas using p-type Si (10^{15} cm^{-3}) resulted in no cathodic shift relative to hematite/fluorine-doped tin oxide (FTO) devices.

For the dual-absorber system to work, the two photon-to-charge conversion processes must take place in a concerted fashion. To this end, we carried out a set of experiments to prove the dual-absorber nature of these devices using monochromatic light for excitation. First, a UV lamp (λ = 365 nm) was used to illuminate the device at relatively low power (3 mW cm^{-2}). These UV photons have sufficient energy to excite hematite, and therefore, most of them were absorbed within hematite itself rather than penetrating through to the Si. The resulting J–V

dx.doi.org/10.1021/ja3051734 | J. Am. Chem. Soc. 2012, 134, 12406–12409

curve and representative band diagram are shown in purple in Figure 3a. When hematite alone is excited, photogenerated

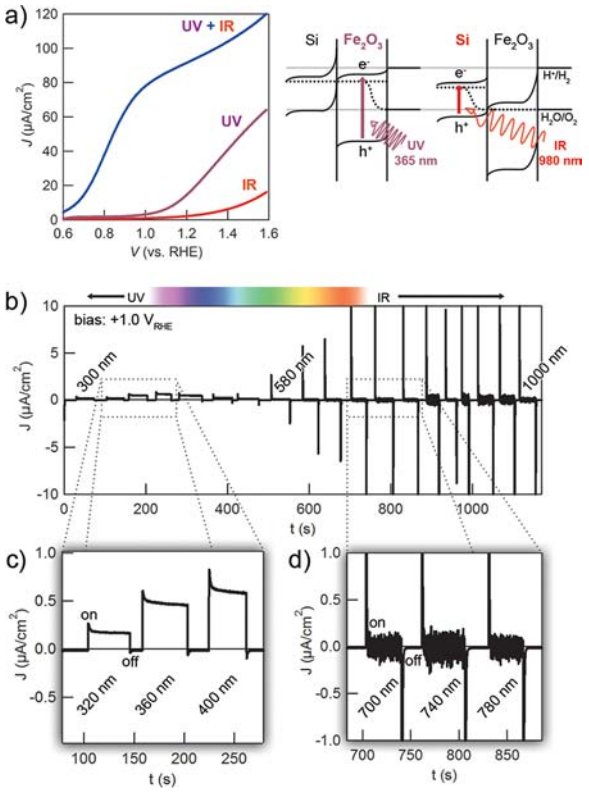

Figure 3. (a) $J-V$ curves for a typical electrode under different and combined monochromatic illumination. (b) Photocurrent responses under stepwise monochromatic light with λ in the range 300−1000 nm under an applied bias of 1.0 V_{RHE}. Magnified views of the UV and IR regions are shown in (c) and (d), respectively.

electrons flow toward Si, where they encounter a barrier that prevents their flow. This results in charge accumulation but no net current flow through the device until a sufficient anodic bias is applied to allow electrons to tunnel through to the Si conduction band (CB). The resulting onset potential of ∼1.0 V_{RHE} reflects the performance expected for a hematite-only device with no significant contribution from Si.

Conversely, when an IR laser (λ = 980 nm) was used as the lone light source, the photons had insufficient energy to excite hematite and instead passed through to be absorbed by Si. Despite the high IR laser power (∼2000 mW cm^{-2}), no appreciable photocurrent was observed until a considerable anodic potential was applied, with only small photocurrents emerging at bias voltages above 1.2 V_{RHE} (Figure 3a, red). This occurred because photoexcited holes in Si cannot be annihilated by electrons from the hematite CB and because they do not have sufficient energy to be injected into hematite and perform water oxidation without a large anodic bias.

However, combining the two light sources for simultaneous illumination of the hematite/Si NW device created a synergistic effect that resulted in full development of the photopotential and cathodic shift of the onset potential. The $J-V$ curve (Figure 3a, blue) shows that in fact the combination of the two single-wavelength light sources is capable of producing a curve shape similar to that obtained under full-solar-spectrum illumination (Figure 1b), albeit with a lower photocurrent magnitude because of the bottleneck in hematite caused by the use of low-power UV illumination. For the case of dual excitation, the band diagram in Figure 1a portrays the cathodic shift of the bands of each n-type material under illumination and the electronic current flow that is produced. The synergy produced by combining the UV and IR illumination sources illustrates the dual-absorber nature of the hematite/Si NW photoelectrode. This clearly contrasts with the single-absorber mechanism of typical hematite/FTO devices, wherein only the UV illumination elicited a photocurrent response (Figure S3c). It also distinguishes our results from those of studies in which Si is the lone active photoanode material, with hematite acting in a passivating[16] or catalytic[17] role.

As further evidence of the device response to photon energy, we measured the wavelength-dependent photocurrent using monochromatic light with 300 nm < λ < 1000 nm under an applied bias of 1.0 V_{RHE}. The illumination was achieved by passing simulated solar light (AM 1.5 spectrum; intensity adjusted to 100 mW cm^{-2}) through a monochromator. The photocurrent response (Figure 3b) reflected the behavior predicted by the $J-V$ curves and band diagrams in Figure 3a. In the short-λ range (300−580 nm) where the primary absorber is hematite, appreciable anodic photocurrent was observed. Since the photocurrent was nonzero, the photoexcited electrons in hematite reached the external circuit, meaning that under this applied anodic bias, photoexcited electrons from the hematite CB can be injected into Si to produce a stable photocurrent. In stark contrast, no net current flow was observed in the long-λ region (580−1000 nm). Also different from the photocurrents measured under short-λ illumination was the apparent noise level, which in the long-λ region was significantly higher. We suggest that this "noisy" current is due to random collection of photogenerated electrons and holes, both from Si. This occurs because the photogenerated hole transfer through hematite into water is forbidden because of the lack of high-energy photons and the large energy barrier to the hematite VB.

We next emphasize two additional features of the chronoamperometry plot shown in Figure 3b, namely, the way the photocurrent levels change and the unique transient behaviors. To present these features more clearly, magnified views of the currents in two spectral regions, 320−400 nm and 700−780 nm, are replotted in Figure 3c,d, respectively. Figure 3c shows that the photocurrent first increased with increasing λ. This trend tracks the abundance of photons in the solar spectrum within this region. For λ > 440 nm, however, the photocurrent decreased as a result of poorer light absorption by hematite at longer λ.[3c,5] The net photocurrent was diminished at 580 nm and beyond, as discussed in the previous paragraph.

The second feature concerns the obvious transient phenomenon that was manifested in the form of current spikes when the light was switched on and off. To explain the nature of these transient spikes, it is necessary to clarify that the anodic photocurrent of an electrode is a measure of how fast *electrons* are collected. An anodic spike in the chronoamperometry plot thus indicates a surge of electrons and is often explained by the charging and discharging effect of trap states.[18] For the hematite/Si NW system, these transient spikes could originate from different groups of trap states: those at the hematite−electrolyte interface[19] or those at the hematite−Si interface. By performing control experiments on hematite/FTO substrates under similar conditions (Figure S5), we concluded that while the transient behaviors under UV and blue illumination may be explained by the nature of the hematite−electrolyte interface, those under red and near-IR illumination can only be explained by charging and

dx.doi.org/10.1021/ja3051734 | J. Am. Chem. Soc. 2012, 134, 12406−12409

discharging of the hematite−Si interface. That is, when the light is switched on, rapid charge separation takes place within Si, with electrons being collected to produce an anodic photocurrent and holes moving to the Si−hematite interface to be trapped there. When these trapped holes recombine with photogenerated electrons from hematite, which takes place under dual-illumination conditions as in Figure 1, a steady-state photocurrent is measured; in the absence of effective photocharge generation within hematite, however, the initial photocurrent quickly decays to the base level (zero net current), resulting in a transient spike. When the light is switched off, annihilation of the initially trapped holes requires electron back-transfer into Si, leading to a cathodic photocurrent spike. This feature can be clearly observed in Figure 3d.

Of course, obtaining a detailed understanding of the transient behaviors, including the kinetics and magnitude, will require additional effort and should yield more useful information (e.g., from impedance characterizations).[19a] Nevertheless, our initial analysis presented above supports the conclusion that the hematite−Si interfaces are preferable sites for photogenerated holes (from Si) and electrons (from hematite) to recombine. Such recombination enables forward current flow and is critically important for the realization of the dual-absorber-based "Z scheme" shown in Figure 1a.

In conclusion, we have shown that when high-quality hematite is deposited on Si NWs in a conformal fashion, hematite and Si can be independently excited by photons in the solar spectrum having different energies. Under simultaneous excitation, a dual-absorber mechanism develops. Charge flow is enabled only when the two absorbers are excited in a synergistic manner, and the photopotentials developed within the two materials contribute to enhanced water splitting performance, as evidenced by a cathodic shift in the photocurrent onset potential. The onset potential of 0.6 V_{RHE} represents one of the lowest reported for hematite photoanode devices and was achieved without the use of catalysts, hematite doping, or surface treatments. These results point out a promising direction for improving the utility of hematite by using direct coupling with small-band-gap materials to utilize the solar spectrum more efficiently and to enhance the photovoltages attainable by a single device. The device fabrication depends on the growth of high-quality thin films of hematite made possible by the ALD technique. Furthermore, the fact that the active materials are primarily composed of three of the four most abundant elements in Earth's crust (O, Si, and Fe) offers promise that renewable energy harvesting by PEC water splitting remains an achievable goal.

■ ASSOCIATED CONTENT

Supporting Information

Experimental details and additional results. This material is available free of charge via the Internet at http://pubs.acs.org.

■ AUTHOR INFORMATION

Corresponding Author

dunwei.wang@bc.edu

Notes

The authors declare no competing financial interest.

■ ACKNOWLEDGMENTS

We thank the NSF (DMR 1055762) for financial support, Y. Lin and G. Yuan for technical assistance, and J. Bisquert, S. G. Julia, and F. F. Santiago for insightful discussions.

■ REFERENCES

(1) (a) Fujishima, A.; Honda, K. *Nature* **1972**, *238*, 37. (b) Pleskov, Y. V. *Solar Energy Conversion: A Photoelectrochemical Approach*; Springer: New York, 1990. (c) Grätzel, M. *Nature* **2001**, *414*, 338. (d) Youngblood, W. J.; Lee, S. H. A.; Maeda, K.; Mallouk, T. E. *Acc. Chem. Res.* **2009**, *42*, 1966. (e) Walter, M. G.; Warren, E. L.; McKone, J. R.; Boettcher, S. W.; Mi, Q.; Santori, E. A.; Lewis, N. S. *Chem. Rev.* **2010**, *110*, 6446. (f) Kronawitter, C. X.; Vayssieres, L.; Shen, S.; Guo, L.; Wheeler, D. A.; Zhang, J. Z.; Antoun, B. R.; Mao, S. S. *Energy Environ. Sci.* **2011**, *4*, 3889.

(2) (a) Sivula, K.; Le Formal, F.; Grätzel, M. *ChemSusChem* **2011**, *4*, 432. (b) Lin, Y.; Yuan, G.; Sheehan, S.; Zhou, S.; Wang, D. *Energy Environ. Sci.* **2011**, *4*, 4862. (c) Martinson, A. B. F.; DeVries, M. J.; Libera, J. A.; Christensen, S. T.; Hupp, J. T.; Pellin, M. J.; Elam, J. W. *J. Phys. Chem. C* **2011**, *115*, 4333.

(3) (a) Lindgren, T.; Wang, H. L.; Beermann, N.; Vayssieres, L.; Hagfeldt, A.; Lindquist, S. E. *Sol. Energy Mater. Sol. Cells* **2002**, *71*, 231. (b) Kay, A.; Cesar, I.; Grätzel, M. *J. Am. Chem. Soc.* **2006**, *128*, 15714. (c) Lin, Y.; Zhou, S.; Sheehan, S. W.; Wang, D. *J. Am. Chem. Soc.* **2011**, *133*, 2398.

(4) Zhong, D. K.; Sun, J.; Inumaru, H.; Gamelin, D. R. *J. Am. Chem. Soc.* **2009**, *131*, 6086.

(5) Lin, Y.; Xu, Y.; Mayer, M. T.; Simpson, Z. I.; McMahon, G.; Zhou, S.; Wang, D. *J. Am. Chem. Soc.* **2012**, *134*, 5508.

(6) Brillet, J.; Cornuz, M.; Formal, F. L.; Yum, J.-H.; Grätzel, M.; Sivula, K. *J. Mater. Res.* **2010**, *25*, 17.

(7) Khaselev, O.; Turner, J. A. *Science* **1998**, *280*, 425.

(8) Reece, S. Y.; Hamel, J. A.; Sung, K.; Jarvi, T. D.; Esswein, A. J.; Pijpers, J. J.; Nocera, D. G. *Science* **2011**, *334*, 645.

(9) Hwang, Y. J.; Boukai, A.; Yang, P. D. *Nano Lett.* **2009**, *9*, 410.

(10) (a) Le Formal, F.; Tétreault, N.; Cornuz, M.; Moehl, T.; Grätzel, M.; Sivula, K. *Chem. Sci* **2011**, *2*, 737. (b) Hisatomi, T.; Le Formal, F.; Cornuz, M.; Brillet, J.; Tétreault, N.; Sivula, K.; Grätzel, M. *Energy Environ. Sci* **2011**, *4*, 2512. (c) Spray, R. L.; McDonald, K. J.; Choi, K.-S. *J. Phys. Chem. C* **2011**, *115*, 3497.

(11) (a) Zhong, D. K.; Gamelin, D. R. *J. Am. Chem. Soc.* **2010**, *132*, 4202. (b) Zhong, D. K.; Cornuz, M.; Sivula, K.; Grätzel, M.; Gamelin, D. R. *Energy Environ. Sci.* **2011**, *4*, 1759. (c) McDonald, K. J.; Choi, K.-S. *Chem. Mater.* **2011**, *23*, 1686.

(12) Cesar, I.; Sivula, K.; Kay, A.; Zboril, R.; Grätzel, M. *J. Phys. Chem. C* **2009**, *113*, 772.

(13) Lehmann, V.; Foll, H. *J. Electrochem. Soc.* **1990**, *137*, 653.

(14) Lin, Y.; Zhou, S.; Liu, X.; Sheehan, S.; Wang, D. *J. Am. Chem. Soc.* **2009**, *131*, 2772.

(15) Yuan, G. B.; Aruda, K.; Zhou, S.; Levine, A.; Xie, J.; Wang, D. W. *Angew. Chem., Int. Ed.* **2011**, *50*, 2334.

(16) Morisaki, H.; Ono, H.; Dohkoshi, H.; Yazawa, K. *Jpn. J. Appl. Phys.* **1980**, *19*, L148.

(17) Jun, K.; Lee, Y. S.; Buonassisi, T.; Jacobson, J. M. *Angew. Chem., Int. Ed.* **2012**, *51*, 423.

(18) (a) Duffy, N. W.; Peter, L. M.; Rajapakse, R. M. G.; Wijayantha, K. G. U. *Electrochem. Commun.* **2000**, *2*, 658. (b) Jennings, J. R.; Ghicov, A.; Peter, L. M.; Schmuki, P.; Walker, A. B. *J. Am. Chem. Soc.* **2008**, *130*, 13364.

(19) (a) Klahr, B.; Gimenez, S.; Fabregat-Santiago, F.; Hamann, T. W.; Bisquert, J. *J. Am. Chem. Soc.* **2012**, *134*, 4294. (b) Cowan, A. J.; Barnett, C. J.; Pendlebury, S. R.; Barroso, M.; Sivula, K.; Grätzel, M.; Durrant, J. R.; Klug, D. R. *J. Am. Chem. Soc.* **2011**, *133*, 10134.